Site-Directed Rotational Resonance Solid-State NMR Distance Measurements Probe Structure and Mechanism in the Transmembrane Domain of the Serine Bacterial Chemoreceptor†

Binumol Isaac,‡ Greg J. Gallagher, Yael S. Balazs,§ and Lynmarie K. Thompson*

Department of Chemistry, University of Massachusetts, Amherst, Massachusetts 01003-9336

Received September 10, 2001

ABSTRACT: The serine receptor of bacterial chemotaxis is an ideal system in which to investigate the molecular mechanism of transmembrane signaling. Solid-state nuclear magnetic resonance (NMR) techniques such as rotational resonance provide a means for measuring local structure and ligand-induced structural changes in intact membrane proteins bound to native membrane vesicles. A general site-directed biosynthetic ^{13}C labeling strategy is used to direct the distance measurements to a specific site; the distance is measured between a unique Cys residue and a non-unique, low-abundance residue (Tyr or Phe). A $^{13}C-^{13}C$ internuclear distance measurement from $^{13}CO(i)$ to $^{13}C\beta(i + 3)$ at the periplasmic edge of the second membrane-spanning helix (TM2) of 5.1 ± 0.2 Å is consistent with the predicted α-helical structure and thus demonstrates an accurate long-distance rotational resonance measurement in the 120 kDa membrane-bound receptor. These measurements require a correction for the rotational resonance exchange between the multiple labels of the non-unique amino acid and the natural-abundance ^{13}C, which is critical to distance measurements in complex systems. A second $^{13}C-^{13}C$ distance measurement between the transmembrane helices provides a high-resolution measurement of tertiary structure in the transmembrane region. The measured 5.0−5.3 Å distance in the presence and absence of ligand is consistent with structural models for the transmembrane region and a proposed signaling mechanism in which ligand binding induces a 1.6 Å translation of TM2. This approach can be used for additional measurements of the structure of the transmembrane region and to determine whether the ligand-induced motion is indeed propagated through the transmembrane helices.

The fundamental biological process of communication across a membrane barrier in a cell, mediated by protein sensors, has been extremely difficult to characterize because of current limitations in biophysical methods when dealing with large protein systems embedded in membranes. Signal transduction by transmembrane receptors is thought to occur by either ligand-induced oligomerization (*1*, *2*), ligand-induced conformational change (*3*, *4*), or some combination of the two. The bacterial chemotaxis receptor family (reviewed in refs *3* and *5*) is composed of homologous proteins that transduce signals about environmental chemoeffectors across the inner membrane. The signal regulates the autophosphorylation activity of a histidine kinase to enable bacteria to direct their swimming behavior toward higher concentrations of attractants or away from repellents. The sequence conservation among these receptors (*6*) and the construction of functional chimeric receptors from domains of different receptors (*7*−*9*) suggest that the bacterial chemotaxis receptors share a similar structure and mechanism. Functional chimeric receptors have also been constructed from the periplasmic ligand binding domain of the aspartate chemotaxis receptor and the intracellular domain of the insulin receptor (*10*, *11*), which suggests these receptors operate by a general mechanism of transmembrane signaling among prokaryotic and eukaryotic receptors. Thus, the well-studied receptors of bacterial chemotaxis are ideal systems for probing the general mechanism of transmembrane signaling.

The structure of the 120 kDa homodimeric chemotaxis receptors (Figure 1a) consists of a periplasmic domain which contains the ligand binding site at the homodimer interface, two membrane-spanning helices, and a cytoplasmic domain which interacts with downstream chemotaxis proteins. High-resolution structural information comes largely from studies of soluble fragments of the receptors. The crystal structures of the ligand-binding domain of the Asp receptor reveal a homodimer of two four-helix bundles (*4*, *12*). The crystal structure of a cytoplasmic fragment of the Ser receptor consists of another four-helix bundle formed by a coiled coil from each monomer (*13*). Cysteine cross-linking studies of the intact receptor have led to low-resolution structural models of the packing of the four helices (TM1,[1] TM2, TM1′, and TM2′) of the transmembrane domain (*14*−*16*) and have

† This research was supported by U.S. Public Health Service Grant GM47601, an award from Research Corp., and an NSF Young Investigator Award. B.I. and Y.S.B. were partially supported by National Research Service Award T32 GM08515 from the National Institutes of Health.

* To whom correspondence should be addressed. E-mail: thompson@chem.umass.edu. Phone: (413) 545-0827. Fax: (413) 545-4490.

‡ Current address: Pharmaceutical Discovery Division, Abbott Laboratories, Abbott Park, IL 60064.

§ Current address: Faculty of Chemistry, 228 Chemistry Bldg., Technion, Haifa 76100, Israel.

10.1021/bi015759h CCC: $22.00
Published on Web 02/08/2002

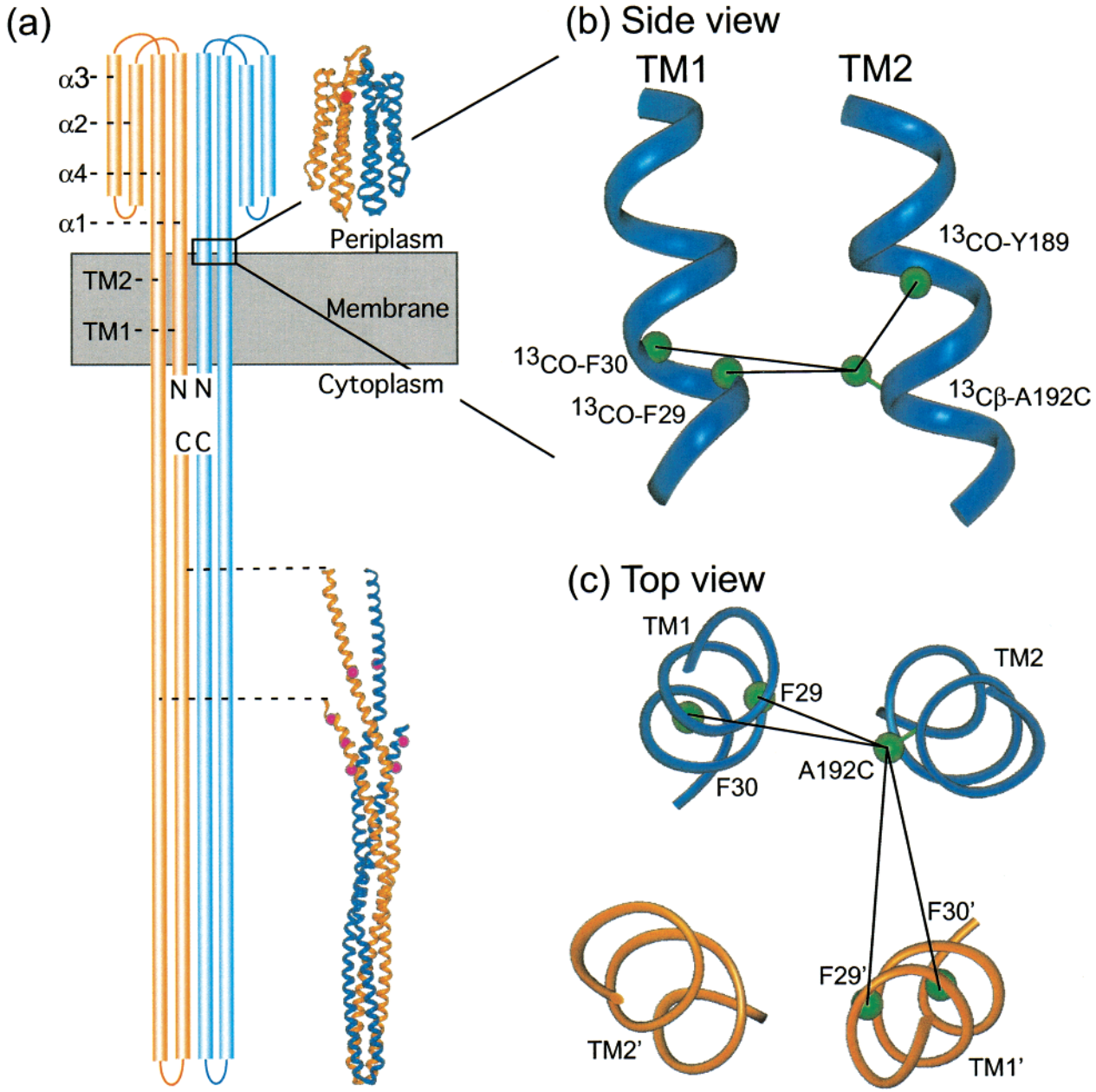

FIGURE 1: Structural overview of bacterial chemotaxis receptors and sites of distance measurements in the intact, membrane-bound serine receptor. (a) Model structure of the Ser receptor (*13*) with helices represented as cylinders. The crystal structures of receptor fragments are shown alongside the corresponding regions. The red ball on the periplasmic domain structure (1vlt) represents the ligand; the dark pink balls on the cytoplasmic domain structure (1qu7) represent the sites which are methylated during adaptation. (b) Side view of helices TM1 and TM2 in the boxed region depicting the target site at A192C and distance vectors from Cβ 192 on TM2 to Tyr189 on TM2 (intrahelical) and to Phe29 and Phe30 on TM1 (interhelical). (c) Top-down view of the boxed region for both monomers depicting the interhelical distance vectors from Cβ 192 on TM2 to Phe29 and Phe30 on both TM1 and TM1′. Structures in panel b and c were drawn using the Kim model coordinates.

also provided evidence for helical structure throughout most of the protein connecting TM2 to the crystallized cytoplasmic fragment (*17*, *18*). Thus, the crystal structures have been joined together by extension of the helices into an elongated helical model of the intact serine receptor (*13*).

Ligand-induced conformational changes are thought to play an important role in the mechanism of transmembrane signaling by bacterial chemotaxis receptors. Comparisons of the crystal structures of the aspartate receptor ligand-binding domain fragment in the presence and absence of ligand have resulted in two different, specific models for transmembrane signaling: a ligand-induced 4° "scissoring" motion across the dimer interface (*4*, *12*) or a 1.6 Å "swinging piston" motion of α4/TM2 relative to α1/TM1 within a subunit (*19*). ^{19}F NMR studies of a soluble ligand-binding fragment of the Asp receptor show ligand-induced chemical shift changes

[1] Abbreviations: CP, cross-polarization; DL, doubly labeled (Phe or Tyr and Cys labeled); IPTG, isopropyl thio-β-D-galactoside; MAS, magic angle spinning; NMR, nuclear magnetic resonance; REDOR, rotational echo double resonance; RR, rotational resonance; SDS−PAGE, sodium dodecyl sulfate−polyacrylamide gel electrophoresis; SD, standard deviation; SL, singly labeled (Phe or Tyr labeled); TM, transmembrane; tsr, Ser receptor gene.

only for ^{19}F-labeled residues probing the α4−α1 interface and not the α1−α1 interface, consistent with a ligand-induced motion of α4 (*20*). Oxidative disulfide cross-linking studies of both the Asp and ribose/galactose receptors suggest the α1/TM1−α1′/TM1′ interface is static (cross-links do not perturb function, and ligand binding does not alter cross-linking). Cross-links across the α1/TM1−α4/TM2 interface perturb signaling in a pattern consistent with a ligand-induced motion of TM2 toward the cytoplasm (*5* and references therein). Finally, EPR studies of spin-labeled Asp receptor samples have detected small line width changes in a pattern consistent with the piston model (*21*, *22*). Overall, these studies have provided low- and high-resolution information about the initiation of the ligand-induced structural change in the periplasmic fragment but only low-resolution information about the propagation of this change through the transmembrane helices. A detailed understanding of the signaling mechanism will require a method for high-resolution structural measurements on intact receptors for following the signal through the transmembrane helices and cytoplasmic domain.

Applying traditional approaches of protein structure determination to membrane proteins is difficult and frequently impractical. High-quality crystals of the membrane−protein complexes for X-ray diffraction are difficult to obtain, and solution NMR determination of complete structures is made difficult by the slow tumbling of the membrane−protein complexes. Solid-state NMR is emerging as an effective tool for studying membrane proteins, because crystals and rapid isotropic tumbling are not required. In solution NMR, rapid tumbling averages dipolar interactions to zero and chemical shifts to an isotropic value, generating narrow resonances. In solid-state NMR spectra of static or slowly tumbling molecules, these interactions are not averaged, which results in broad NMR resonances with low resolution and sensitivity. Both resolution and sensitivity can be improved by using isotopic labeling, combined with either sample orientation with respect to the magnetic field or magic angle spinning (MAS). Complete high-resolution structure determination of small membrane peptides such as gramicidin A has been accomplished using oriented samples (*23*). Local structure and mechanistic questions have been addressed in membrane proteins such as bacteriorhodopsin using MAS experiments (*24*). The MAS approach has benefited from the development of several solid-state NMR techniques which selectively reintroduce and measure dipolar couplings to obtain structural information (for reviews on homonuclear and heteronuclear dipolar recoupling methods, see refs *25* and *26*).

Site-directed solid-state NMR distance measurements using the above MAS recoupling techniques are a powerful approach for mapping local structure and structural changes in proteins. Our laboratory has used site-directed REDOR to measure a heteronuclear (^{13}C−^{19}F) distance between helices α1 and α4 in the periplasmic domain of the intact Ser receptor (*27*). The measured ligand-induced distance change is potentially consistent with the piston model, and further measurements in the vicinity are in progress to map the actual motion in the intact, membrane-bound receptor.

Here we report site-directed distance measurements in the transmembrane domain of the Ser receptor which aim to refine the low-resolution structural model and to follow the propagation of the ligand-induced change in conformation. These experiments have employed rotational resonance (RR) (*28*) to measure homonuclear (^{13}C−^{13}C) distances. Initial attempts were hampered by several experimental problems. One of these problems was resolved by the introduction of a new constant time RR method suited for long distance measurements (*29*). We have further refined the RR methodology to correct for the contribution of the natural-abundance ^{13}C in a multiply labeled system, which is critical to distance measurements in complex systems. We have measured three ^{13}C−^{13}C distances in different signaling states of the serine receptor bound to native bacterial inner membrane vesicles. A measurement of the directly bonded ^{13}CO−^{13}Cα distance of the 35 glycines in the receptor tests a known distance in the membrane−protein system. A CO(i)−Cβ(i + 3) distance measurement at the periplasmic edge of TM2 is consistent with α-helical secondary structure and demonstrates the accuracy of a long distance measurement in the receptor. Finally, a measurement of an interhelical (TM1−TM2′) distance within the transmembrane domain provides a direct measurement of helix packing contacts. The latter two distance measurements were targeted using site-directed mutagenesis to introduce a unique Cys residue and were measured in the presence and absence of ligand to probe whether ligand-induced conformational changes extend into the transmembrane domain of the receptor. The successful site-directed RR distance measurements in a complex system provide an additional tool for mapping signaling mechanisms involving ligand-induced conformational change.

MATERIALS AND METHODS

Chemicals. Labeled compounds were all 99% ^{13}C, from Cambridge Isotope Laboratories. Zinc acetate was synthesized according to the following protocol (K. V. Lakshmi, personal communication). Powdered zinc metal (0.05 mol) and acetic acid (0.2 mol) were refluxed in a double-neck round-bottom flask with stirring at ∼120 °C for a couple of days; the color changed from gray to white. The solid product was dissolved in hot EtOH and hot water and then cooled. The solvent was removed by rotary evaporation, and crystals formed when the flask was scratched with a glass rod. The crystals were filtered with a medium fritted glass filter and dried at 37 °C. The melting temperature and NMR spectrum were checked to verify the synthesized product. Natural-abundance and doubly ^{13}C-labeled zinc acetate were synthesized separately, mixed in a 1:1 ratio, and doped with 3% (w/w) manganese acetate to shorten the T_1 relaxation time.

Strains and Plasmids. The serine receptor overexpression plasmid pHSe5.tsr (*30*, *31*), a gift of F. W. Dahlquist (University of Oregon, Eugene, OR), was the template for construction of the mutant receptor. The QuikChange method (Stratagene) was utilized to introduce the A192C point mutation in the wild-type tsr gene (*32*). Sequencing results verified the presence of the desired mutation and the absence of any errors in the full tsr sequence. Swarm assays were performed in *Escherichia coli* strain HCB429 [relevant genotype, Δ*(tsr)7021,* Δ*(tar-tap)5201,* Δ*(tar)100, zbd*::Tn5] (*33*). Overexpression for isolation of Ser receptor-containing inner membrane vesicles was performed in *E. coli* strain DL39C (relevant genotype, *cysE::Tn5, aspC13, fnr-25, ilv12, tyrB507*). DL39C is auxotrophic for both cysteine and

phenylalanine along with other residues [Tyr, Asp, Leu, Ile, and Val (leaky)]. DL39C was constructed from DL39CM (*metE::Tn10, cysE::Tn5, aspC13, fnr-25, ilv12, tyrB507*), a generous gift from D. LeMaster (Wadsworth Center, Albany, NY). To eliminate the tetracycline resistance, Tn10 was removed from DL39CM using Met^-, chlortetracycline, fusaric acid plates (in the presence of kanamycin to retain Cys auxotrophicity), which capitalize on the toxicity of fusaric acid to cells with tetracycline resistance (*34*). Overexpression levels of pHSe5.tsr and pHSe5.tsrA192C in the resulting DL39C strain were excellent, provided that kanamycin was not included in the medium during induction. Retention of the Cys and Phe auxotrophies was verified by innoculating 20 μL of an overnight cell culture (OD_{600} = 1.3) grown in the absence of kanamycin into 2 mL cultures of defined media with all the Cys/Phe combinations (C^+F^+, C^+F^-, C^-F^+, or C^-F^-); only the C^+F^+ medium supported cell growth.

Swarm Assays. Chemotaxis swarm assays were performed as described in ref *27* on HCB429/pHSe5.tsr, HCB429/pHSe5.A192Ctsr, and HCB429/pUC9. The inoculated swarm plates (with or without 100 μM L-serine) were allowed to sit for 12−15 h at room temperature and then placed in the incubator at 37 °C. The swarm diameters were measured at 2 h intervals for the next 8−10 h with the first measurement set equal to time zero. Each reported time point was the average of three equivalent swarm ring diameter measurements. The swarming due to serine was determined from the difference in swarm diameters in the presence and absence of serine. The nearly negligible diameters measured for HCB429/pUC9, which does not express the Ser chemotaxis receptor, were subtracted from the above difference to give the final measurement at each time point. Plots of swarm diameters versus time were used to determine the swarm rate (slope of the line).

Isolation of Ser Receptor-Containing Inner Membrane Vesicles. Cultures of DL39C cells transformed with pHse5.tsr plasmids were grown overnight at 30 °C in 1 L cultures of defined medium (*30*) containing 100 μg/mL ampicillin. For NMR sample preparation, the differently labeled samples (DL, doubly labeled, Phe or Tyr and Cys labeled; SL, singly labeled, Phe or Tyr labeled; and UL, unlabeled) were grown in parallel 1 L cultures in most cases. The cultures were supplied with [1,2-$^{13}C_2$]glycine (550 mg/L), L-[$^{13}C\beta$]cysteine (25 mg/L), L-[^{13}CO]phenylalanine (50 mg/L), or L-[1-^{13}C]-tyrosine (50 mg/L), or with equivalent amounts of the corresponding unlabeled amino acids as appropriate. The auxotrophicity of DL39C for Phe, Tyr, and Cys ensured complete (99%) labeling of these amino acids. Cells were grown at 28−30 °C with 250 rpm vigorous shaking. Receptor expression was induced at an OD_{600} of 0.3−0.4 with 500 μM IPTG for 3 h.

Inner membrane vesicles were prepared following the protocol of Gegner et al. (*31*). Cells were harvested by centrifugation for 15 min at 4000 rpm in a Sorvall 1 L volume rotor at 4 °C. Each cell pellet was resuspended to $^1/_{20}$ of the original volume in 30% (w/w) sucrose and 10 mM Tris (pH 8.0). The doubly labeled (DL) cultures were combined and then divided into two fractions to make the with Ser and without Ser samples. L-Serine (2 mM) was added to one fraction and was included in all subsequent buffers to ensure the presence of 2 mM serine on both sides of the resulting vesicles. All fractions were kept on ice for 40 min after addition of 100 μg/mL hen egg white lysozyme and 5 mM EDTA (final concentrations). Formation of spheroplasts was initiated by slowly diluting the cells with 2 volumes of a solution containing 1 mM 1,10-phenanthroline, 5 mM EDTA, and 1 mM PMSF to inhibit proteolysis. A fast dilution with an additional 4 volumes of water and stirring for 10 min caused osmotic lysis of cells to form separate inner and outer membrane vesicles. The total membrane fraction was collected by centrifugation at 10 000 rpm in a Beckman JA 20 rotor for 3 h with subsequent resuspension and homogenization in ~15 mL (per pellet) of 30% (w/w) sucrose, 10 mM Tris (pH 8.0), and 5 mM EDTA buffer. The homogenized pellet was loaded onto a sucrose gradient of 55, 50, and 40% (w/w) sucrose, all with 5 mM EDTA, for overnight centrifugation in a Beckman SW 28 rotor at 28 000 rpm. The large middle band between the 50 and 55% sucrose layers was collected and dialyzed overnight against 20 mM phosphate buffer (pH 7.3) with or without 2 mM Ser to remove residual sucrose (1 L of phosphate buffer per 1 L of original cells with two or three buffer changes).

The total protein yield (determined by the BCA assay) was ~40 mg/L of original cells. A visual estimate of the percentage of Ser receptor out of the total proteins was ~50−60%. The dialyzed inner membrane vesicles were pelleted by ultracentrifugation at 45 000 rpm (Beckman Ti70 rotor) and packed into the 4 mm NMR rotor as a wet pellet. NMR samples were ~25 mg of total protein.

The overexpressed receptor preparations were tested for abnormal protein aggregation in a detergent solubilization assay under conditions that fully solubilize chemotaxis receptors expressed at wild-type levels. Total protein (2 mg/mL) was incubated on ice for 30 min with 1% β-octyl glucoside and then pelleted at 24 psi (~90000*g*) in a Beckman airfuge for 1 h. Comparison of the supernatant and unspun fractions by SDS−PAGE showed that typical Ser receptor preparations were >75% solubilized by this protocol, for cell cultures grown at 28−30 °C.

Oxidative disulfide formation, used for verification of the presence of Cys in the mutant receptor and for assigning the cysteine Cβ shift in the NMR spectrum, was catalyzed by Cu(II)(1,10-phenanthroline)$_3$ in the presence of ambient dissolved O_2. Conditions chosen for the highest degree of cross-linking (assessed by SDS−PAGE under nonreducing conditions) were 10 μM receptor incubated with 1% Cu-(phen)$_3$ for 20 min at 37 °C.

Ligand Binding Assays. Ligand binding affinities of the receptor preparations were tested using a [^{3}H]Ser displacement assay (*35*, *36*) performed as described in ref *27*. The data ($[Ser]_{bound}$ vs $[Ser]_{total}$) were fit to the 1:1 binding equation to obtain the two parameters K_d and $[R]_{total}$. The concentration of the receptor dimer ($[R]_{total}$) which resulted from the fit was consistent with the BCA assay and purity estimate.

NMR Spectroscopy and Data Analysis. Cross-polarization magic angle spinning (CPMAS) experiments were performed on a Bruker ASX300 spectrometer utilizing a 4 mm Bruker high-speed MAS probe operating at frequencies of 300.13 (^{1}H) and 75.47 MHz (^{13}C). The magic angle spinning speed controller keeps spinning rate fluctuations to less than ±3 Hz. ^{13}C chemical shifts were calibrated to the 31 ppm methyl peak of 1,4-di-*tert*-butylbenzene (vs TMS at 0 ppm).

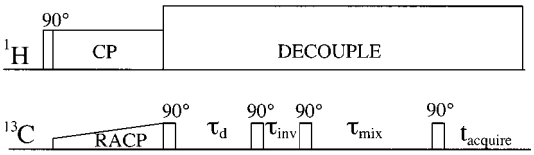

FIGURE 2: Constant time rotational resonance pulse sequence. Homonuclear dipolar coupling is reintroduced by spinning at the rotational resonance condition, where $\upsilon_r = \Delta\sigma_{iso}$ (see Materials and Methods). A ramped CP enhances carbon sensitivity. A delay with spins on the *z*-axis (τ_d) is used to achieve a constant decoupling time for all mixing times. Selective inversion is achieved by the $90-\tau_{inv}-90$ sequence. Magnetization exchange occurs during a variable mixing time (τ_{mix}) after which spins are put into the *xy* plane for detection.

NMR spectra were collected at low temperatures ($T_{read\ out} \sim 230$ K, $T_{sample} \sim 245$ K) to avoid protein denaturation during long experimental runs and to reduce motion, thereby increasing CP efficiency. Dry air for the spinning and cooling gases was supplied from a Balston Instrument air dryer. The bearing air was passed through two sets of copper coils, both immersed in chilled cryocool fluid (Savant Instruments, Inc.). The first bath was cooled by a CC-100II immersion cooler (NESLAB Instruments) to approximately −70 °C; the second bath was cooled by dry ice. The second bath was necessary to maintain the receptor samples frozen with the frictional heating by the rapid MAS and the rf heating by the long high-power proton decoupling times. The reflected power on the ^{1}H and ^{13}C channels was monitored during spectral acquisition to check for any increases that might indicate detuning upon sample thawing.

Rotational resonance [RR (*28*)] reintroduces homonuclear dipolar interactions by spinning at the rotational resonance condition where $n\upsilon_r = \Delta\sigma_{iso}$. The MAS speed was set to the $n = 1$ condition, where the magic angle spinning speed (υ_r) is equal to the difference in isotropic chemical shifts ($\Delta\sigma_{iso}$) between the resonances to be recoupled, for maximum magnetization exchange. Ramped CP (*37*) was used to maximize CP efficiency at the high spinning speeds needed for RR (≈12 kHz), and was optimized to obtain a CO:CH$_2$ ratio of 1:1 for a natural-abundance glycine standard at the desired spinning speed for each RR experiment. CP times of 1.5−2.5 ms were used with a 16% ramp on the ^{13}C channel. The constant time RR pulse sequence with a time delay inversion [Figure 2 (*29*)] was used for maximum efficiency and reliability of long distance measurements. This sequence incorporates a variable period (τ_d), first suggested by Tomita et al. (*38*), before the time delay inversion, that changes in proportion to the mixing time (τ_{mix}) so that each mixing time experiment experiences the same length of proton decoupling and thus the same degree of rf heating ($\tau_d + \tau_{mix} = 10$ ms for the Gly experiments and 60 ms for the Tyr/Cys and Phe/Cys experiments). Selective inversion was achieved by placing both spins into the *xy* plane and waiting [$\tau_{inv} = (2\Delta\sigma_{iso})^{-1}$], with the carrier frequency midway between the resonances to be recoupled, to let the spins precess 180° apart, followed by another ^{13}C 90° pulse to put the spins onto $\pm z$ for RR exchange during τ_{mix}. ^{1}H and ^{13}C 90° pulse lengths of 5 μs were used ($\gamma B_1/2\pi = 50$ kHz), and the proton power level was increased to ∼69 kHz (Gly and Phe/Cys experiments) or 100 kHz (Tyr/Cys experiments) during rotational resonance and acquisition times. Residual magnetization left in the *xy* plane by misset and/or imperfect 90° pulses was canceled by a 128 phase cycle. To minimize signal variations due to instrumental drift over long signal averaging times, spectra were collected by cycling through several mixing times with 128 scans recorded per mixing time. Optimized rotational resonance solid-state NMR parameters were verified using zinc [1,2-^{13}C$_2$]acetate to obtain results that matched published spectra (*28*).

Rotational resonance spectra were collected for a range of mixing times for the two doubly labeled samples (DL with or without Ser) and a singly labeled (SL) sample, and for one or two mixing times for an unlabeled (UL) sample. Previous work (*29*) and control experiments (not shown) show that the unlabeled sample RR spectrum does not change with mixing time. Parallel preparations of the labeled and unlabeled samples gave the cleanest difference spectra (minimized the subtraction artifacts). Comparison of two different samples always requires a scaling factor to correct for differences in sample size. These factors (c_1 and c_2) were chosen by equalizing the Cα resonance between the DL and UL samples (DL = $c_1 \times$ UL) and equalizing the carbonyl resonance between the DL and SL sample (DL = $c_2 \times$ SL). Consistent scaling parameters were applied to each set of RR experiments.

Magnetization exchange curves, used to determine the distances, are obtained by plotting the decay of the difference magnetization ($I_1 - I_2$) versus mixing time. For the [1,2-^{13}C$_2$]Gly labeled receptor experiments, where the exchange with natural abundance is negligible, $I_1 - I_2$ was measured by integration in DL − UL difference spectra. We have recently developed a method for correcting for the natural-abundance contribution to the RR exchange and applied this method to analyze the Phe/Cys experiment (*32*). For this analysis, RR spectra of the DL and SL samples were combined to make a $(DL - SL)_t$ series of difference spectra that give the exchange additional to natural-abundance exchange at each mixing time. Since this subtraction nulls the carbonyl resonance (carbonyl label is in both DL and SL samples), the intensity of a single carbonyl is added back as $(1/n)(SL - UL)_{0ms}$, where n is the number of labeled carbonyl residues per protein. Thus, for the case of 13 Phe residues, the series $(DL - c_2 \times SL)_t + (1/13)(c_2 \times SL - c_1 \times UL)_0$ can be used to measure $I_1 - I_2$ (*32*). We have now developed an improved approach which uses mostly difference spectra between different mixing times obtained on the same sample (comparable to the REDOR ΔS spectrum), which are therefore free of difference artifacts and give a clear picture of the magnitude and position of the RR exchange. The full intensity of the sites of interest is measured in the $(DL - c_1 \times UL)_0$ spectrum, and the DL − SL RR exchange is subtracted from this as follows: $I_1 - (1/n)I_2$ in $(DL - c_1 \times UL)_0$ minus $I_1 - I_2$ in $DL_{0-t} - c_2 \times SL_{0-t}$. This method was chosen because the Tyr/Cys spectra were difficult to match between samples; scaling factors chosen to match the carbonyls of the DL and SL spectra gave a poor match of the aliphatic region leading to a negative artifact in DL − SL difference spectra which reduced the intensity of the Cys resonance. Such artifacts disappear in difference spectra obtained on the same sample. In addition, the DL_{0-t} and SL_{0-t} spectra should be antisymmetric ($I_1 + I_2 = 0$), because for RR exchange $I_1 + I_2$ is constant (*39*), providing a rapid qualitative assessment of the experiment.

Peak intensities were measured by integration. The integration regions were centered at the chemical shifts of maximum RR exchange for the desired site, which are the peak maxima of the DL(0−60 ms exchange) difference spectrum (174.5 and 24.5 ppm). Narrow integration limits (a 5 ppm range centered on the peak) were chosen to avoid including difference artifacts (visible in the DL − UL spectrum). Inclusion of such artifacts could increase the 0 ms peak intensities with a component not undergoing exchange, and thus decrease the apparent extent of exchange and overestimate the distance. The error of the intensity measurements in each spectrum was estimated from the noise, measured in a signal-free region of the spectrum (103−111 ppm). The error of a peak height is the standard deviation of the noise, σ. The error of an integral is $\sigma \times i \times \sqrt{n}$, where i is the integration interval (1 for all cases) and n is the number of points integrated. An au program, areasd, was written to calculate peak heights, integrals, and standard deviations within the Bruker XWINNMR software. The errors were propagated through calculations of the normalized difference magnetization.

Simulations of rotational resonance magnetization exchange curves for various distances, $I_{CH_2} - I_{CO}$ versus τ_{mix}, were generated using the rsq2spin program (*40*), which is similar to the cc2z program (*39*) but also takes chemical shift dispersion into account. Line widths used in the simulations were as follows: $\Delta\nu_{1/2}^{CO} = 590$ Hz and $\Delta\nu_{1/2}^{CH_2} = 450$ Hz for 35 glycines, from spectra off of the rotational resonance spinning condition. For the long distance experiments (Tyr/Cys and Phe/Cys, with dipolar coupling being less than the line width), off-RR spectra are not needed since there should be no detectable rotational resonance-induced broadening. For the unique Cys Cβ, the line width in the DL − UL spectrum was used, ∼250 Hz for the Tyr/Cys experiment (100 kHz decoupling) and ∼325 Hz for the Phe/Cys experiment (70 kHz decoupling). For the non-unique site, the line width in the DL(0−60 ms exchange) spectrum for the site participating in the RR exchange was used, because the DL − UL spectrum should be an overestimate (corresponds to 9 Tyr or 13 Phe residues rather than the single site of interest). Carbonyl line widths of ∼180 and ∼240 Hz were observed for the Tyr and Phe resonances, respectively, in the DL(0−60 ms exchange) spectra. The DL − UL line widths were slightly larger for 13 unresolved Phe residues (∼315 Hz). The somewhat resolved resonance for the nine Tyr CO groups (in the DL − UL spectrum) was deconvoluted into three components, corresponding to roughly one Tyr residue at 171 ppm, five Tyr residues at 174 ppm, and three Tyr residues at 177 ppm. The RR MAS was chosen to match the central, dominant component (with chemical shift corresponding to helical structure). The 180 Hz line width of this component was consistent with the line width in the DL(0−60 ms exchange) spectrum.

T_2 measurements are needed to estimate T_2^{ZQ}, an important parameter for the rotational resonance magnetization exchange simulations. T_2^{ZQ} cannot be estimated from line widths for these studies because of the large chemical shift dispersion expected due to labeling of multiple sites. Instead, it is estimated using the relation $(T_2^{ZQ})^{-1} = (T_2^{CO})^{-1} + (T_2^{CH_2})^{-1}$. T_2 measurements used a ramped CP followed by a standard $\tau-180-\tau-$AQ sequence with rotor synchronization and the same ^{1}H decoupling fields used for rotational resonance ($\gamma B_1/2\pi \sim 70$ and 100 kHz). A T_2^{CO} of 8.0 ms and a $T_2^{C\alpha}$ of 4.5 ms for [1,2-$^{13}C_2$]glycine powder were obtained, which match the observed line widths of 40 and 70 Hz, respectively, as expected for a polycrystalline powder with little or no chemical shift dispersion. For the 35 [1,2-$^{13}C_2$]glycine in the serine receptor, $T_2^{CO} = 3.0$ ms and $T_2^{C\alpha} = 1.7$ ms, predicting that $T_2^{ZQ} = 1.1$ ms. However, the T_2^{ZQ} of 2.0 ms was found to provide a better fit to the data. For the Tyr/Cys experiments with a decoupling field of 100 kHz, $T_2^{CO} = 9.4$ ms and $T_2^{C\beta} = 5.0$ ms, predicting that $T_2^{ZQ} = 3.3$ ms. For the Phe/Cys experiments with a decoupling field of 70 kHz, $T_2^{CO} = 7.2$ ms and $T_2^{C\beta} = 1.7$ ms, predicting that $T_2^{ZQ} = 1.4$ ms. Chemical shift anisotropy and asymmetry parameters were based on published glycine values (*41*): $\delta_{CO} = 5510$ Hz, $\eta_{CO} = 0.95$, $\delta_{CH_2} = 1510$ Hz, and $\eta_{CH_2} = 0.95$. The Euler angles relating each CSA tensor to the dipolar tensor are unknown; values of (0,0,0) were used, and varying this parameter had no detectable effect on exchange curves for these $n = 1$ experiments.

For the Tyr/Cys and Phe/Cys measurements, the best-fit distance and its precision were determined using nonlinear least-squares fitting of the rotational resonance data. For rapid fitting of the data, a simple function was chosen which reproduces the shape of the exact rsq2spin simulations for weak dipolar couplings:

$$y = 1 + A[\exp(-t/b) - 1]$$

Values of A were chosen so that the function matched the rsq2spin simulated exchange curves for our system in the appropriate distance range ($A = 0.54$ and 0.61 for the Tyr/Cys and Phe/Cys experiments, respectively). One-parameter fits to the data yielded best fit and standard deviation values for the parameter b; curves plotted for $b \pm$ SD were matched visually to rsq2spin simulation curves to obtain the corresponding distances. The curves plotted in Figures 7 and 9 are the matching rsq2spin simulations. The ±1 SD error bars for the $I_1 - I_2$ data are smaller than the data symbols in all cases and are omitted on the plots for clarity. These errors are calculated from the spectral noise and do not include the error introduced by matching different samples, which is likely to be larger. When these errors were used for the fitting, the resulting error in the distance was unrealistically small (≪0.1 Å). Each data point within these RR experiments should have approximately the same error [same number of scans were acquired, and (unlike REDOR) no T_2 relaxation decreases the signal at long mixing times]. Thus, we chose not to use the underestimated error bars to weight the data for the fitting, and found that the unweighted fits gave larger, more realistic errors, which are reported.

RESULTS

[1,2-$^{13}C_2$]Gly Directly Bonded Distance in the Serine Receptor. Biosynthetic labeling with [1,2-$^{13}C_2$]Gly introduces directly bonded carbon labels at 35 glycine sites per monomer of the serine receptor. This provides the opportunity to test the accuracy of a rotational resonance distance measurement on receptor samples with a known distance independent of protein structure. Spectra of unfrozen receptor samples have significantly lower signals than those of frozen samples,

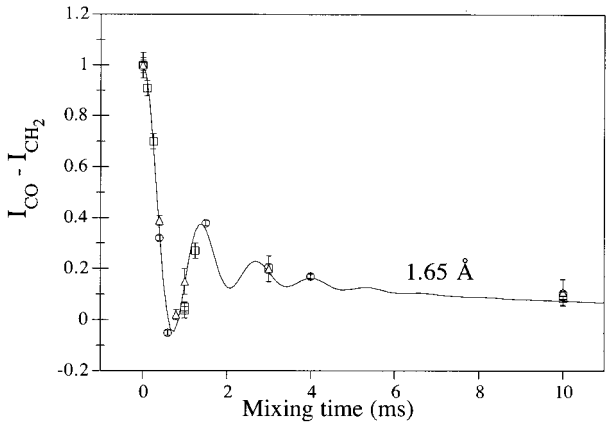

FIGURE 3: [1,2-$^{13}C_2$]Glycine serine receptor rotational resonance magnetization exchange. Difference magnetization values ($I_{CO} - I_{CH_2}$), determined by peak areas in DL − UL difference spectra, are plotted as a function of mixing time for rotational resonance exchange at −23 (○), 5 (△), and −13 °C (□). The simulated curve (solid line) is for a 1.65 Å internuclear distance (other parameters described in Materials and Methods), which is slightly longer than the α-glycine crystal structure distance of 1.52 Å. Error bars represent the standard deviation of the sum magnetization values ($I_{CO} + I_{CH_2}$), which should remain constant.

presumably due to motion reducing the cross-polarization efficiency. Thus, experiments on unfrozen receptor samples are possible for the 35 glycines but impractical for the site-directed distance measurements described below, which observe a single carbon in the 60 kDa, membrane-bound protein. Rotational resonance measurements on frozen samples require greater cooling than for REDOR measurements; it is important to be sure that the longer decoupling time and higher spinning speed do not cause the sample to thaw during the experiment. Figure 3 shows the rotational resonance magnetization exchange data ($I_1 - I_2$ vs mixing time) for three different experiment temperatures (5, −13, and −23 °C). The fact that similar data are obtained over a temperature range of nearly 30 °C suggests that motions which would attenuate the dipolar coupling are not occurring (at least for the portion of the sample detected in CP spectra). The experimental fit to the 1.65 Å simulation curve (solid line) shows that the measured dipolar coupling is slightly longer than the 1.52 Å distance determined from the crystal structure of glycine (*42*). Previous solid-state NMR internuclear distance measurements suggest that 10% attenuation of the dipolar coupling occurs due to high-frequency motions, which would predict a corresponding distance of 1.58 Å. Thus, the accuracy of a short distance measurement in the membrane-bound Ser receptor system is ∼0.1 Å, and rotational resonance distance measurements on membrane vesicles containing the intact Ser receptor are feasible.

Mutagenesis for Site-Directed Distance Measurements. A site-directed distance measurement strategy was designed to target distance measurements to specific sites in the 120 kDa homodimeric serine receptor. Since the wild-type Ser receptor has no Cys residues, site-directed mutagenesis of a single residue was used to introduce a unique Cys for subsequent biosynthetic labeling and distance measurements probing the structure and signaling mechanism. An Ala to Cys mutation at position 192 in TM2 (Figure 1) was chosen to allow two distance measurements, one dependent solely on secondary structure and the other probing tertiary structure and proposed conformational change mechanisms involving motions across the TM1−TM2 interface. Selection of this site was based on the Pakula model for the structure of the transmembrane region [based on disulfide cross-linking of cysteine residues (*14*)]. The model predicts measurable distances between this unique site and two relatively low-abundance amino acids (13 Phe and 9 Tyr residues per monomer). For the secondary structure measurement, the A192C $^{13}C\beta$−Tyr189 ^{13}CO distance was predicted to be ∼4.4 Å for a CO(i)−Cβ($i + 3$) distance in a typical α-helix. For the tertiary structure measurement, the interhelical distances from A192C $^{13}C\beta$ were predicted to be 4.1 or 4.0 Å to Phe30 ^{13}CO and 6.2 or 5.4 Å to Phe29 ^{13}CO (TM1−TM2′ or TM2−TM1′ interface, respectively) in the Pakula model of the aspartate receptor transmembrane domain. This site has the advantage of having two nearby phenylalanines, increasing the chances of finding a measurable interhelical distance despite the limitations of a low-resolution model.

The A192C site was also chosen for its ability to test a variety of proposed signaling mechanisms. Modeling (InsightII, Molecular Simulations, Inc., San Diego, CA) based on the proposed piston motion (*19*) applied to the Pakula structure predicts that a 1.6 Å translation of TM2′ relative to TM1 would change the closest interhelical distance at the target site from 4.0 to 2.9 Å, a change that clearly can be detected by the rotational resonance experiment. In addition, if this interhelix contact spans the dimer interface as predicted, it is sensitive to conformational changes between subunits, such as proposed scissors (*12*) or rotation (*43*) models.

A cysteine was introduced in the Ser receptor at position 192 using site-directed mutagenesis. The presence of the A192C mutation in the Ser receptor was verified by sequencing of the gene and with a disulfide cross-linking gel assay of the expressed protein. Swarm rates and ligand binding affinities were measured to check the functionality of the mutant receptors (*32*). The swarm assay, which tests the overall bacterial response to ligand, shows similar rates of swarming for the wild-type receptor (0.85 ± 0.01 mm/h) and the A192C mutant receptor (0.97 ± 0.02 mm/h). Radioactive ligand displacement assays were performed to measure the binding affinity for serine. The results for the A192C receptor (K_d = 38 ± 12 μM) are comparable to dissociation constants reported in the literature for the wild-type Ser receptor (5−27 μM) (*36, 44*). These assays indicate the A192C receptor is functional.

Assignment of the Unique Cysteine $^{13}C_\beta$ NMR Resonance. Observation of the singly labeled $^{13}C\beta$ Cys in NMR spectra of the 60 kDa A192C Ser receptor is difficult due to overlap with the 1% natural-abundance ^{13}C resonances of the protein and lipids. Difference spectra of matched labeled and unlabeled samples (grown and isolated in parallel) typically have difference artifacts of comparable magnitude to the signal of interest. For example, the difference spectrum shown in Figure 4b has two aliphatic resonances at 15 and 24 ppm. The reported range of chemical shifts for Cys Cβ in proteins is 22−57 ppm [Restricted Set of Amino Acid Chemical Shifts in the BMRB (www.bmrb.wisc.edu) as of February 2001]. Thus, the 24 ppm resonance is likely to be the Cys Cβ, and disulfide cross-linking was used to verify this assignment. An I195C receptor sample was split into two fractions which were treated in parallel either with or

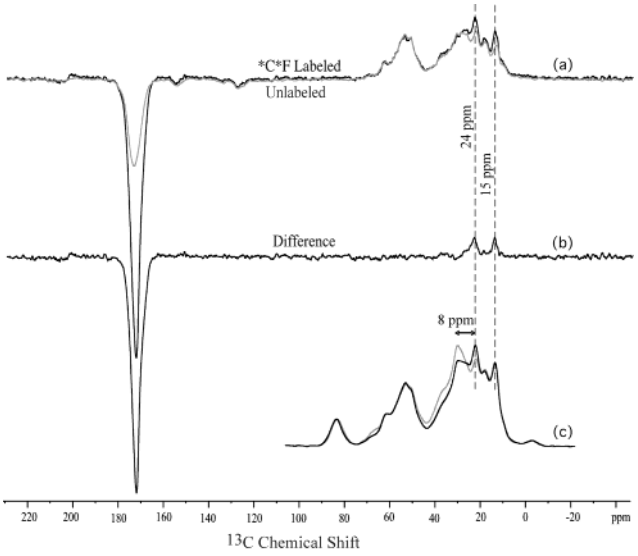

FIGURE 4: ^{13}C spectra of ^{13}CO Phe, ^{13}Cβ Cys192 labeled serine receptors. There are 13 tyrosines and 1 cysteine in the receptor. (a) Doubly labeled (DL, black) and unlabeled (UL, gray) spectra are superimposed. (b) The labeled minus unlabeled difference spectrum (DL − UL) shows the prominent ^{13}CO resonance of the 13 Phe residues at 173 ppm and two possible resonances for ^{13}Cβ Cys at 24 and 15 ppm. (c) The aliphatic region of the spectra of non-cross-linked (black) and cross-linked (gray) samples are superimposed (ω_r = 6.6 kHz; 31 000 scans per spectrum). Only the 24 ppm peak shifts upon cross-linking and is thus assigned to Cys Cβ. The 15 ppm peak is a persistent difference artifact.

without Cu(phen)$_3$. Comparison of the two fractions by gel electrophoresis demonstrates that a large fraction of the receptor is cross-linked by Cu(phen)$_3$ oxidation (*32*). Figure 4c compares the ^{13}C NMR spectra of the cross-linked and the non-cross-linked receptor samples. Cross-linking results in an 8 ppm downfield shift of the 24 ppm resonance to 32 ppm, and no change in the 15 ppm resonance. An 8 ppm downfield shift is also observed in a comparison of spectra of pure ^{13}Cβ cysteine and ^{13}Cβ cystine powders, with resonances at 27 and 35 ppm, respectively. Thus, we assign the 24 ppm resonance to the unique cysteine in the protein.

Natural-Abundance ^{13}C Contribution to Rotational Resonance of Multiply Labeled Proteins. The site-directed RR strategy aims to measure the distance between a unique amino acid (Cys introduced by mutagenesis) and a non-unique amino acid (13 Phe or 9 Tyr residues in this study). Because of the multiple labeling of the non-unique amino acid, the natural-abundance ^{13}C background can make a significant contribution to the rotational resonance magnetization exchange, which must be corrected with appropriate control experiments. The rotational resonance exchange between the single ^{13}Cβ Cys192 and natural-abundance ^{13}C carbonyls is likely to be small; complete exchange with one nearby ^{13}CO (at 1% abundance) would reduce the ^{13}Cβ intensity by only 1%. However, the presence of 13 Phe or 9 Tyr ^{13}CO labels makes it possible to have significant ($\approx$10 times more) exchange with natural-abundance ^{13}C at 24 ppm, reducing the peaks by $\approx$10%, an amount comparable to a long distance measurement.

The magnitude of this natural-abundance effect is illustrated for the case of Phe labeling by comparing rotational resonance exchange in doubly labeled (DL), singly labeled (SL), and unlabeled (UL) receptor samples. Figure 5 compares the full rotational resonance exchange (0 ms exchange minus 60 ms exchange) for (a) ^{13}CO Phe, ^{13}Cβ Cys192C Ser receptor (DL), (b) ^{13}CO Phe Ser receptor (SL), and (c) unlabeled Ser receptor (UL). The three spectra are scaled before subtraction, by equalizing the aromatic peak to correct for sample size differences. The lack of rotational resonance exchange in spectrum c indicates that there is no significant exchange between natural abundance at 174 ppm and natural abundance at 24 ppm, as expected. There is, however, significant exchange between labeled Phe ^{13}CO and natural abundance at 24 ppm (SL sample, Figure 5b). In the presence of the ^{13}Cβ Cys192 label (DL sample, Figure 5a), the magnitude of the exchange increases by only a very small amount, indicating that there is only a small rotational resonance exchange between ^{13}CO Phe and the Cys192 site. This suggests that ^{13}Cβ Cys192 is much further than the predicted 4.0 Å from the carbonyl carbons of both Phe29 and Phe30. Furthermore, measurement of this distance will require that the RR exchange be measured on both the ^{13}CO Phe, ^{13}Cβ Cys192C Ser receptor (DL) and ^{13}CO Phe Ser receptor control sample (SL). Such SL control experiments are needed for any rotational resonance study involving a multiply labeled site, and are included below in the rotational resonance experiments on both the ^{13}CO Tyr, ^{13}Cβ Cys192C and ^{13}CO Phe, ^{13}Cβ Cys192C Ser receptor samples.

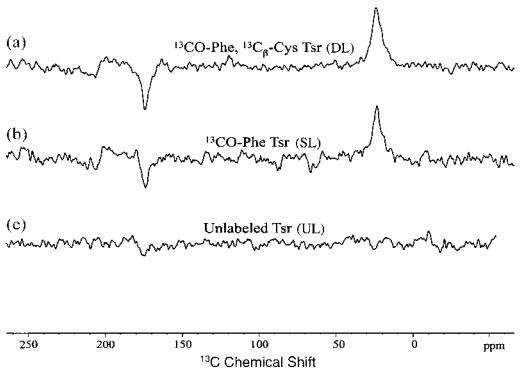

FIGURE 5: Magnetization exchange in the doubly labeled, singly labeled, and unlabeled Ser receptor. RR magnetization exchange difference spectra (mixing time of 0−60 ms) in (a) ^{13}CO Phe, ^{13}Cβ Cys192 receptor (DL), (b) ^{13}CO Phe Ser receptor (SL), and (c) unlabeled (UL) Ser receptor samples demonstrates the large magnitude of exchange of 13 labeled carbonyls with natural abundance at 24 ppm (spectrum b).

Protein and lipid components of the sample can account for the exchange observed in SL samples with natural-abundance peaks. The magnitude of the natural-abundance exchange in an SL sample is predictable for the simple case of rotational resonance exchange with the natural-abundance protein resonance at 51 ppm (due to protein Cα) in a lipid-free region of the spectrum. The intensity change in the CO resonance is 0.13 of the total 13 Phe residues, consistent with complete exchange of each of the 13 Phe ^{13}CO groups with the 1% ^{13}C in the directly bonded Cα (*32*). The exchange with natural abundance at 24 and 15 ppm appears to involve the lipid component of the sample. The ^{13}C natural-abundance spectrum of *E. coli* lipids shows an abundance of resonances between 10 and 30 ppm, including resonances at 24 (CH_2) and 15 ppm (CH_3). The magnitude of rotational resonance magnetization exchange of the 13

Table 1: Rotational Resonance Data for the ^{13}CO Tyr, $^{13}C\beta$ Cys Labeled A192C Serine Receptor

$I_1 - {}^1/_9 I_2$ in $(DL - c_1 \times UL)_0$			$I_1 - I_2$ in $(DL_{0-t} - c_2 \times SL_{0-t})$		normalized $I_1 - I_2$[a]	
without Ser	with Ser	mixing time (ms)	without Ser	with Ser	without Ser	with Ser
8.197	5.108	0	0	0	1.000 ± 0.001	1.000 ± 0.001
		15	1.824	1.099	0.778 ± 0.001	0.785 ± 0.002
		30	1.948	1.489	0.762 ± 0.002	0.709 ± 0.002
		45	0.700	1.263	0.915 ± 0.002	0.753 ± 0.002
		60	2.490	1.489	0.696 ± 0.002	0.708 ± 0.006

[a] Normalized $I_1 - I_2 = [I_1 - {}^1/_9 I_2$ in $(DL - c_1 \times UL)_0$ minus $I_1 - I_2$ in $(DL_{0-t} - c_2 \times SL_{0-t})]/[I_1 - {}^1/_9 I_2$ in $(DL - c_1 \times UL)_0]$, where $c_1 = 1.15$ and $c_2 = 1.68$ (sample without Ser) and $c_1 = 0.98$ and $c_2 = 1.32$ (sample with Ser). Error estimated from spectral noise is likely to be underestimated, since it does not include errors in matching samples.

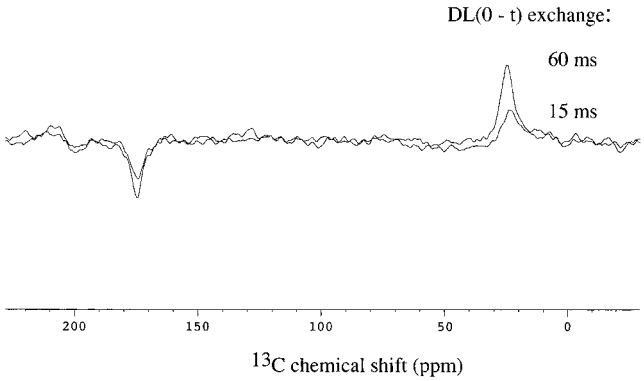

FIGURE 6: Rotational resonance difference spectra of the ^{13}CO Tyr, $^{13}C\beta$ Cys192 Ser receptor. DL_{0-t} difference spectra for 15 and 60 ms of magnetization exchange show increasing peak intensities due to RR exchange (ω_r = 11.294 kHz; 25 472 scans per spectrum).

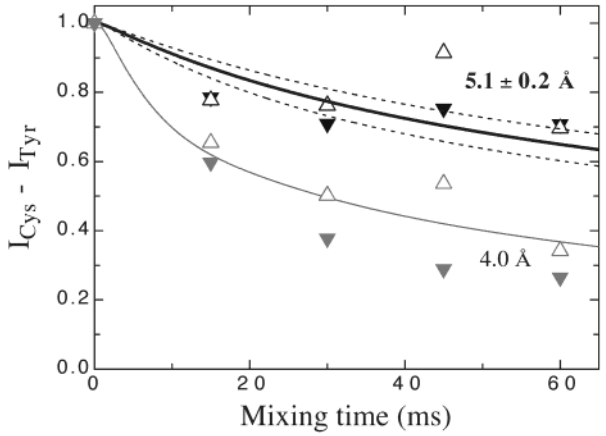

FIGURE 7: Rotational resonance magnetization exchange plot for the Tyr189 ^{13}CO−Cys192 $^{13}C\beta$ distance measurement. Difference magnetization values ($I_{Cys} - I_{Tyr}$) data are plotted vs mixing times for receptor without Ser (△) and receptor with Ser (▼). These data show good agreement between experiments on two different samples. The simulated curves for the best fit (solid) and ±one standard deviation (dashed) of 5.1 ± 0.2 Å for both samples are plotted. The data and 4.0 Å curve shown in gray, which are uncorrected for the RR exchange of the multiple Tyr with natural abundance in the SL sample, demonstrate the importance of making this correction.

^{13}CO Phe residues with the 15 ppm natural-abundance resonance in an SL sample is smaller than the exchange with the 24 ppm resonance, consistent with the smaller magnitude of the 15 ppm peak in the lipid spectrum. Exchange with the 15 ppm peak is ~2-fold greater for 45 ^{13}CO Leu residues than for 13 ^{13}CO Phe residues, which correlates with the frequency of occurrence of the residue in the membrane [11 Leu vs 5 Phe residues (*32*)]. Thus, the exchange with natural abundance at 24 and 15 ppm is likely to involve the lipid resonances.

Tyr189 ^{13}CO−Cys192 $^{13}C\beta$ Intrahelical Distance in the Serine Receptor. As a test of the accuracy of the RR measurement of a long distance in the receptor, with the natural-abundance correction, we measured a CO(i)−Cβ(i + 3) distance from Tyr189 ^{13}CO to Cys192 $^{13}C\beta$. This distance is predicted to be 4.2 Å for a classical α-helix, and for the helical residues in the Asp receptor periplasmic domain (1vls), the CO(i)−Cβ(i + 3) distance is 4.4 ± 0.4 Å (average ± SD). Thus, we expect a distance of 4.0−4.8 Å which should not be changed by ligand binding.

To correct for the exchange of the 9 Tyr ^{13}CO groups with the natural abundance at 24 ppm, rotational resonance spectra were collected for both DL (^{13}CO Tyr, $^{13}C\beta$ Cys) and SL (^{13}CO Tyr) samples of the A192C Ser receptor. The unlabeled (UL) sample spectra were identical for 0 and 60 ms of magnetization exchange, as expected. Figure 6 compares DL_{0-t} spectra for 15 and 60 ms. As discussed in Materials and Methods, the spectra are free of difference artifacts because they are differences of two spectra on the same sample, and show the full extent of RR exchange in the DL sample (exchange in SL must still be subtracted).

The magnetization exchange data (Table 1), plotted as $I_1 - I_2$ versus mixing time in Figure 7, demonstrate good agreement with the known distance and reproducibility between different samples. The corrected data (in black) are comparable for the receptor samples without Ser (△) and receptor samples with Ser (▼). These data (with the exception of the 45 ms point for the sample without Ser, which clearly deviates from all the rest) were fit to an exponential decay function, which was matched to rotational resonance simulation curves to obtain the corresponding distances. For both samples, the fit yielded 5.1 ± 0.2 Å, which demonstrates that the matching and scaling of spectra to make the natural-abundance correction can be done in a consistent manner for different samples. The best-fit distance curve is plotted in Figure 7 (solid black line) along with the ±one standard deviation curves (dashed lines). The magnitude of the correction for exchange of the Tyr with natural abundance at 24 ppm (exchange in the SL sample) is large. The uncorrected data are plotted in gray in Figure 7, along with a 4.0 Å curve corresponding to the best-fit distance for the uncorrected data for samples without Ser. This demonstrates that the correction for exchange with natural abundance is critical for RR involving a multiply labeled site, since omission of this correction would underestimate the distance by ~1 Å both for the Phe/Cys experiment (data not shown)

Table 2: Rotational Resonance Data for the ^{13}CO Phe, $^{13}C\beta$ Cys Labeled A192C Serine Receptor

$I_1 - {}^1/_{13}I_2$ in $(DL - c_1 \times UL)_0$			$I_1 - I_2$ in $(DL_{0-t} - c_2 \times SL_{0-t})$		normalized $I_1 - I_2$[a]	
without Ser	with Ser	mixing time (ms)	without Ser	with Ser	without Ser	with Ser
5.957	6.797	0	0	0	1.000 ± 0.002	1.000 ± 0.001
		20	0.792	1.079	0.867 ± 0.002	0.841 ± 0.002
		40	1.102	1.136	0.815 ± 0.003	0.833 ± 0.002
		60	1.253	2.338	0.790 ± 0.002	0.656 ± 0.002

[a] Normalized $I_1 - I_2 = [I_1 - {}^1/_{13}I_2$ in $(DL - c_1 \times UL)_0$ minus $I_1 - I_2$ in $(DL_{0-t} - c_2 \times SL_{0-t})]/[I_1 - {}^1/_{13}I_2$ in $(DL - c_1 \times UL)_0]$, where $c_1 = 0.57$ and $c_2 = 1.12$ (sample without Ser) and $c_1 = 0.69$ and $c_2 = 1.35$ (sample with Ser). Error estimated from spectral noise is likely to be underestimated, since it does not include errors in matching samples.

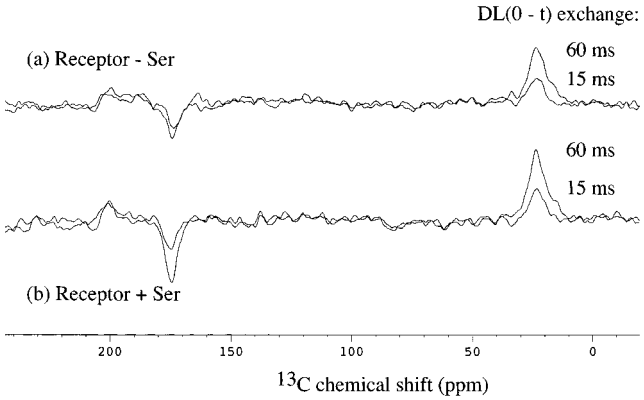

FIGURE 8: Rotational resonance difference spectra of the ^{13}CO Phe, $^{13}C\beta$ Cys192 labeled Ser receptor. (a) DL_{0-t} difference spectra for 15 and 60 ms of magnetization exchange in the ligand-free receptor (20 736 scans per spectrum). (b) DL_{0-t} difference spectra for 15 and 60 ms of magnetization exchange in the ligand-bound receptor (35 072 scans per spectrum). $\omega_r = 11.338$ kHz in both cases.

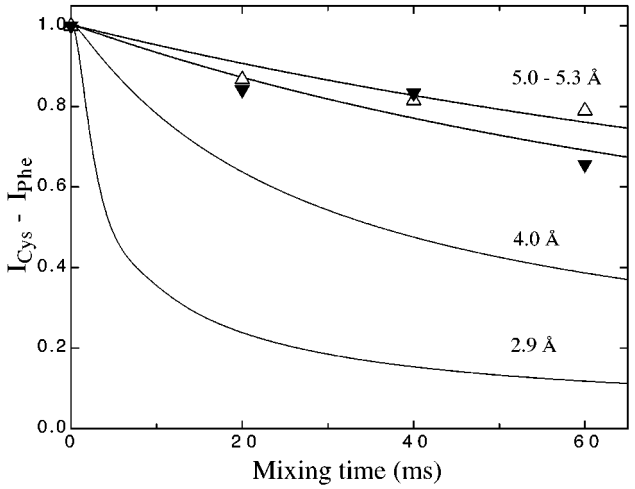

FIGURE 9: Rotational resonance magnetization exchange plot for the Phe29/30 ^{13}CO−Cys192 $^{13}C\beta$ distance measurement. Difference magnetization values ($I_{Cys} - I_{Phe}$) and best-fit distance simulation curves (black curves) are plotted for the receptor without Ser (△, 5.3 Å) and the receptor with Ser (▼, 5.0 Å). These distances are comparable to those predicted in the Kim model of the intact Ser receptor (see Table 3). For comparison, curves are plotted for the predicted distance of 4.0 Å in the Pakula model, and 2.9 Å after a 1.6 Å piston displacement of TM2 in the Pakula model.

and for the Tyr/Cys experiment shown in Figure 7. Finally, the agreement between the measured distance of 5.1 ± 0.2 Å and the expected range of 4−4.8 Å for an α-helix demonstrates the accuracy of rotational resonance for a long distance measurement involving a multiply labeled (non-unique) site in membrane-bound Ser receptor samples.

Phe29/30 ^{13}CO−Cys192 $^{13}C\beta$ Interhelical Distance in the Serine Receptor. To map the structure and ligand-induced structural changes in the transmembrane domain of the receptor, the distance between transmembrane helices TM1 and TM2 was measured in a site-directed RR experiment on the ^{13}CO Phe, $^{13}C\beta$ Cys labeled A192C Ser receptor. Again, RR spectra were collected on DL (^{13}CO Phe, $^{13}C\beta$ Cys) and SL (^{13}CO Phe) samples for equivalent mixing times. Spectra comparing the extent of RR exchange (DL_{0-t}) at 15 and 60 ms for receptor samples both with Ser and without Ser are plotted in Figure 8. The magnetization exchange data ($I_1 - I_2$, Table 2) are plotted versus mixing time in Figure 9 and fit to determine the interhelical distances in the two receptor samples. The plot and the fits indicate there is no significant distance change upon ligand binding; the data for samples without and with Ser correspond to distances of 5.3 ± 0.1 and 5.0 ± 0.1 Å, respectively. The measured distances of 5.0−5.3 Å are significantly longer than the distance of 4.0 Å predicted by the cross-linking model and provide a distance constraint for the transmembrane structure in the intact Ser receptor.

This analysis assumes that a single Phe dominates the RR exchange with Cys192 $^{13}C\beta$. Further experiments could test this assumption and determine the distances to Phe29 and/or Phe30 by using either mutagenesis or an NMR filter to remove the contribution from one of the Phe sites. Such experiments would also test the possibility that the presence of two Phe residues obscured a ligand-induced distance change, for example, if ligand binding happens to lengthen the distance to one Phe while shortening the distance to the other, by amounts which leave the total dipolar coupling unchanged.

DISCUSSION

NMR Methods for Site-Directed Rotational Resonance Distance Measurements in Membrane Proteins. We have demonstrated an accurate site-directed RR measurement of a long distance in the 60 kDa Ser receptor by a general strategy that can be applied to other large membrane proteins. A large body of cross-linking data on chemotaxis receptors (*5*, *16*) are consistent with the idea that TM2 and α4 form a continuous α-helix. The distance of 5.1 ± 0.2 Å we have measured between Tyr189 ^{13}CO and Cys192 $^{13}C\beta$ is consistent with the predicted α-helical structure as this transmembrane helix emerges from the membrane. This demonstrates that a rotational resonance distance measurement in the membrane-bound receptor is accurate, despite the potential inaccuracies due to estimating the T_2^{ZQ} (errors here would likely alter the distance by a few tenths of an angstrom) and due to impurities in the native membrane

Table 3: Predicted and NMR-Measured Distances from A192C Cβ to Phe29 or Phe30 CO

	model distance[a]		
ligand-free state	Pakula model (*14*)	Kim model (*13*)	NMR-measured distance[b]
closest distance	4.0/4.1 Å (Phe30, inter)	5.2/5.6 Å (Phe29, intra)	5.3 Å (without Ser)
other distances	5.4/6.2 Å (Phe29, inter); 12−14 Å (intra)	7.7/8.0 Å (Phe30, intra); 9−10 Å (inter)	
ligand-bound state	distance after 1.6 Å TM2 translation (*19*)[c]		
closest distance	2.9 Å	5.3/5.5 Å	5.0 Å (with Ser)

[a] The two inter- and two intramonomer distances to Phe29 and -30 are listed. [b] The current NMR experiments do not discriminate between whether the measured distance is to Phe29 or Phe30 and whether it is intra- or intermonomer. The NMR analysis assumes a single close Phe and the same distance for both monomers. [c] A pure 1.6 Å translation of TM2 along its axis toward the cytoplasm is applied to the Pakula model and Kim model coordinates. For simplicity, we have omitted the 5° tilt of the proposed swinging piston mechanism (*19*).

samples. The success of these experiments required the constant time rotational resonance experiment (*29*, *38*), maintaining frozen samples despite frictional and rf heating, discrimination of the unique Cys Cβ resonance from difference artifacts, and correction for the exchange of the multiple carbonyl labels with natural-abundance ^{13}C at 24 ppm. The latter correction is required for multiply labeled proteins, and can be quite large; in the case of the ^{13}CO Tyr, ^{13}Cβ Cys receptor, it changed the distance from 4.0 Å without correction to 5.1 Å with correction. To the best of our knowledge, other RR studies in the literature have not yet demonstrated the importance of such a correction. Most RR studies have been performed on synthetic peptides or ligand sites where it is possible to incorporate two unique labels. With site-directed Cys labeling and proper correction for the other multiply labeled non-unique site, RR experiments become a general tool that can be applied throughout large proteins. Thus, both site-directed REDOR (*27*) and RR have been successfully applied to an intact, membrane-bound protein, and these tools for high-resolution measurements of heteronuclear and homonuclear interatomic distances can provide information about structure and mechanism that is unavailable with any other method.

The weakest aspect of both the RR and REDOR experiments on such complex systems is the need to match two different samples to make corrections for natural-abundance contributions to the initial signal intensity and to the exchange (RR) or dephasing (REDOR). Note that this matching introduces an additional error that has not been included in our estimates, which are based solely on spectral noise. Development and application of practical NMR methods utilizing a third label for making the correction within the same sample (*45*) should significantly increase the reliability of these approaches.

Implications for Structure and Transmembrane Signaling Mechanism in the Serine Receptor. This study uses MAS solid-state NMR to measure an interhelical distance in the transmembrane region of an intact, membrane-bound bacterial chemotaxis receptor. The distance of 5.0−5.3 Å between Phe29 or -30 ^{13}CO and Cys192 ^{13}Cβ is the first high-resolution distance constraint for refining structural models of the transmembrane region of bacterial chemotaxis receptors. The Pakula model for the transmembrane helix packing appears to be qualitatively correct, and it enabled us to choose a site of close contact for NMR distance measurements. However, the measured distance of 5.0−5.3 Å is significantly longer than the closest distance of 4 Å predicted by the Pakula model, and appears to be more consistent with the recent model by Kim and co-workers (*13*) which predicts a closest distance of 5.2−5.6 Å. Table 3 summarizes the predicted and measured distances. Additional distance measurements between the transmembrane helices are needed to provide additional constraints to test and refine proposed structural models of the transmembrane region.

Ligand binding does not significantly change the measured interhelical distance. To evaluate whether the measured distances are consistent with the proposed 1.6 Å piston motion of TM2 toward the cytoplasm, we checked the target distance after a 1.6 Å displacement of TM2 in each of the model structures. For the Pakula model, there is a significant distance decrease (from 4 to 3 Å), and for the Kim model, there is essentially no change (5.2−5.3 Å; see Table 3). This demonstrates that the precise geometry has a large impact on the predicted change so that structural refinement is critical to determining which mechanisms are consistent with the NMR-measured distances. In particular, when Phe29 and -30 are above the target site (toward the periplasm) as in the Pakula model, the 1.6 Å piston shortens the target distance. The Kim model has Phe29 and -30 more nearly across from the target site (A192C) so that there would be little distance change upon translation of either helix. If the transmembrane domain structure has a geometry similar to that of the Kim model, the NMR-measured distances are consistent with the proposed ligand-induced 1.6 Å downward piston of TM2. Alternate possibilities are that the ligand-induced motion observed in the periplasmic domain is not propagated through the transmembrane helices or that there is some other motion that does not alter this distance. In summary, our absolute distances of 5.0−5.3 Å between Phe29 or -30 ^{13}CO and Cys192 ^{13}Cβ are more consistent with the Kim model for the intact Ser receptor structure, and are consistent with the proposed 1.6 Å piston model for this geometry.

A recent site-directed REDOR NMR study (*27*) has measured a ligand-induced distance change in the periplasmic domain which is consistent with the proposed piston mechanism of signaling. The currently measured distance in the transmembrane domain does not change upon ligand binding, which, although consistent with the piston model, does not prove that the conformational change is propagated via the transmembrane helices. Additional high-resolution distance measurements are needed to map the local structure at these sites for both signaling states and follow the ligand-induced structural change in the intact, membrane-bound receptor.

This site-directed solid-state NMR approach is complementary to the spin-labeled EPR studies of membrane proteins pioneered by Hubbell and co-workers (*46*) and applied to the Asp receptor (*21*, *22*). Solid-state NMR is

limited to shorter distance measurements and is much less sensitive than EPR, making fewer measurements possible, but the precision is higher. For example, the EPR detection of a conformational change for the aspartate receptor periplasmic domain is limited by the spin-label mobility to 2.5 Å resolution (*21*). In addition, mapping a conformational change of a backbone is difficult if side chain sites of spin-labels could readjust to accommodate changes in the backbone. In contrast, the solid-state NMR approach demonstrated here can directly measure small changes in backbone conformation with a resolution of ~0.2 Å.

Site-directed rotational resonance is a new general strategy for mapping structure and structural changes in membrane proteins and other systems. Solid-state NMR experiments on the Ser receptor are providing important information about ligand-induced structural changes that may play a role in the mechanism of transmembrane signaling. These methods represent a powerful approach for meeting the challenges of understanding mechanisms of other important membrane proteins.

ACKNOWLEDGMENT

We thank Rick Dahlquist for the pHSe5.tsr plasmid, Owen Murphy for help with mutagenesis, and Charlie Dickinson for technical support of the NMR facility. We are grateful to Andy Pakula for the coordinates of his model of the transmembrane helices of the Asp receptor and to Sung-Hou Kim for the coordinates of his model of the intact Ser receptor. We thank Phil Costa, Malcom Levitt, and Bob Griffin for the cc2z (M. Levitt) and rsq2spin (P. Costa) programs for simulations of rotational resonance magnetization exchange, Ed Voigtman for discussions of error analysis, Mike Englehardt (Bruker Instruments) and Frank Kovacs for the areasd au program used in the NMR peak intensity analysis, and Bob Weis for helpful discussions and comments on the manuscript. The NMR instrument was purchased with a grant from the NSF (BIR-911996) and funds from the University of Massachusetts, and is partially supported by the NSF Materials Research Science and Engineering Center Facility at the university.

REFERENCES

1. Lemmon, M. A., and Schlessinger, J. (1994) *Trends Biochem. Sci. 19*, 459−463.
2. Bormann, B. J., and Engelman, D. M. (1992) *Annu. Rev. Biophys. Biomol. Struct. 21*, 223−242.
3. Falke, J. J., Bass, R. B., Butler, S. L., Chervitz, S. A., and Danielson, M. A. (1997) *Annu. Rev. Cell Dev. Biol. 13*, 457−512.
4. Milburn, M. V., Prive, G. G., Milligan, D. L., Scott, W. G., Yeh, J., Jancarik, J., Koshland, D. E., Jr., and Kim, S. H. (1991) *Science 254*, 1342−1347.
5. Falke, J. J., and Hazelbauer, G. L. (2001) *Trends Biochem. Sci. 26*, 257−265.
6. Krikos, A., Mutoh, N., Boyd, A., and Simon, M. I. (1983) *Cell 33*, 615−622.
7. Krikos, A., Conley, M. P., Boyd, A., Berg, H. C., and Simon, M. I. (1985) *Proc. Natl. Acad. Sci. U.S.A. 82*, 1326−1330.
8. Tatsuno, I., Lee, L., Kawagishi, I., Homma, M., and Imae, Y. (1994) *Mol. Microbiol. 14*, 755−762.
9. Weerasuriya, S., Schneider, B. M., and Manson, M. D. (1998) *J. Bacteriol. 180*, 914−920.
10. Moe, G. R., Bollag, G. E., and Koshland, D. E., Jr. (1989) *Proc. Natl. Acad. Sci. U.S.A. 86*, 5683−5687.
11. Biemann, H. P., Harmer, S. L., and Koshland, D. E., Jr. (1996) *J. Biol. Chem. 271*, 27927−27930.
12. Yeh, J. I., Biemann, H. P., Prive, G. G., Pandit, J., Koshland, D. E., Jr., and Kim, S. H. (1996) *J. Mol. Biol. 262*, 186−201.
13. Kim, K. K., Yokota, H., and Kim, S. H. (1999) *Nature 400*, 787−792.
14. Pakula, A. A., and Simon, M. I. (1992) *Proc. Natl. Acad. Sci. U.S.A. 89*, 4144−4148.
15. Lee, G. F., Burrows, G. G., Lebert, M. R., Dutton, D. P., and Hazelbauer, G. L. (1994) *J. Biol. Chem. 269*, 29920−29927.
16. Lynch, B. A., and Koshland, D. E., Jr. (1991) *Proc. Natl. Acad. Sci. U.S.A. 88*, 10402−10406.
17. Butler, S. L., and Falke, J. J. (1998) *Biochemistry 37*, 10746−10756.
18. Danielson, M. A., Bass, R. B., and Falke, J. J. (1997) *J. Biol. Chem. 272*, 32878−32888.
19. Chervitz, S. A., and Falke, J. J. (1996) *Proc. Natl. Acad. Sci. U.S.A. 93*, 2545−2550.
20. Danielson, M. A., Biemann, H. P., Koshland, D. E., Jr., and Falke, J. J. (1994) *Biochemistry 33*, 6100−6109.
21. Ottemann, K. M., Thorgeirsson, T. E., Kolodziej, A. F., Shin, Y. K., and Koshland, D. E., Jr. (1998) *Biochemistry 37*, 7062−7069.
22. Ottemann, K. M., Xiao, W., Shin, Y. K., and Koshland, D. E., Jr. (1999) *Science 285*, 1751−1754.
23. Ketchem, R. R., Hu, W., and Cross, T. A. (1993) *Science 261*, 1457−1460.
24. Lugtenburg, J., Mathies, R. A., Griffin, R. G., and Herzfeld, J. (1988) *Trends Biochem. Sci. 13*, 388−393.
25. Tycko, R. (2001) *Annu. Rev. Phys. Chem. 52*, 575−606.
26. Griffin, R. G. (1998) *Nat. Struct. Biol. 5* (Suppl.), 508−512.
27. Murphy, O. J., III, Kovacs, F. A., Sicard, E. L., and Thompson, L. K. (2001) *Biochemistry 40*, 1358−1366.
28. Raleigh, D. P., Levitt, M. H., and Griffin, R. G. (1988) *Chem. Phys. Lett. 146*, 71−76.
29. Balazs, Y. S., and Thompson, L. K. (1999) *J. Magn. Reson. 139*, 371−376.
30. Muchmore, D. C., McIntosh, L. P., Russell, C. B., Anderson, D. E., and Dahlquist, F. W. (1989) *Methods Enzymol. 177*, 44−73.
31. Gegner, J. A., Graham, D. R., Roth, A. F., and Dahlquist, F. W. (1992) *Cell 70*, 975−982.
32. (Isaac) James, B. (2001) M.S. Thesis, University of Massachusetts, Amherst, MA.
33. Wolfe, A. J., Conley, M. P., Kramer, T. J., and Berg, H. C. (1987) *J. Bacteriol. 169*, 1878−1885.
34. Bochner, B. R., Huang, H. C., Schieven, G. L., and Ames, B. N. (1980) *J. Bacteriol. 143*, 926−933.
35. Biemann, H. P., and Koshland, D. E., Jr. (1994) *Biochemistry 33*, 629−634.
36. Clarke, S., and Koshland, D. E., Jr. (1979) *J. Biol. Chem. 254*, 9695−9702.
37. Metz, G., Wu, X. L., and Smith, S. O. (1994) *J. Magn. Reson., Ser. A 110*, 219−227.
38. Tomita, Y., O'Connor, E. J., and McDermott, A. (1994) *J. Am. Chem. Soc. 116*, 8766−8771.
39. Levitt, M. H., Raleigh, D. P., Creuzet, F., and Griffin, R. G. (1990) *J. Chem. Phys. 92*, 6347−6364.
40. Lansbury, P. T., Costa, P. R., Griffiths, J. M., Simon, E. J., Auger, M., Halverson, K. J., Kocisko, D. A., Hendsch, Z. S., Ashburn, T. T., Spencer, R. G. S., Tidor, B., and Griffin, R. G. (1995) *Nat. Struct. Biol. 2*, 990−998.
41. Veeman, W. S. (1984) *Prog. NMR Spectrosc. 16*, 193−235.
42. Legros, J.-P., and Kvick, Å. (1980) *Acta Crystallogr. B36*, 3052−3059.
43. Cochran, A. G., and Kim, P. S. (1996) *Science 271*, 1113−1116.
44. Lin, L. N., Li, J., Brandts, J. F., and Weis, R. M. (1994) *Biochemistry 33*, 6564−6570.
45. Pan, Y., and Schaefer, J. (1990) *J. Magn. Reson. 90*, 341−345.
46. Hubbell, W. L., Gross, A., Langen, R., and Lietzow, M. A. (1998) *Curr. Opin. Struct. Biol. 8*, 649−656.

BI015759H